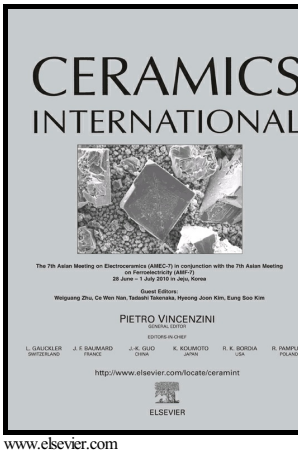

Structural, optical and photodegradation properties of pure and Fe-doped titania nanoparticles probed using simulated Solar light

Milica Carević, Nadica D. Abazović, Tatjana Savić, Tatjana B. Novaković, Miloš D. Mojović, Mirjana I. Čomor

PII: S0272-8842(15)01808-8
DOI: http://dx.doi.org/10.1016/j.ceramint.2015.09.100
Reference: CERI11377

To appear in: *Ceramics International*

Received date: 20 July 2015
Revised date: 15 September 2015
Accepted date: 17 September 2015

Cite this article as: Milica Carević, Nadica D. Abazović, Tatjana Savić, Tatjana B. Novaković, Miloš D. Mojović and Mirjana I. Čomor, Structural, optical and photodegradation properties of pure and Fe-doped titania nanoparticles probed using simulated Solar light, *Ceramics International*, http://dx.doi.org/10.1016/j.ceramint.2015.09.100

Structural, optical and photodegradation properties of pure and Fe-doped titania nanoparticles probed using simulated Solar light

Milica Carević[a], Nadica D. Abazović[a], Tatjana Savić[a], Tatjana B. Novaković[b], Miloš D. Mojović[c], Mirjana I. Čomor[a*]

[a]Vinča Institute of Nuclear Sciences, University of Belgrade, P.O. Box 522, 11000Belgrade, Serbia

[b]IChTM- Department of Catalysis and Chemical Engineering, University of Belgrade, Njegoševa 12, 11000 Belgrade, Serbia

[c]Faculty of Physical Chemistry, University of Belgrade, Studentski trg 12-16,P.O.Box 47, 11158 Belgrade, Serbia

[*]Corresponding authors: Dr Mirjana Čomor: e-mail: mirjanac@vinca.rs, Phone: +381 11 380 41 92; Fax: +381 11 3408 607; Vinča Institute of Nuclear Sciences, University of Belgrade, P.O. Box 522, 11001 Belgrade, Serbia.

Abstract

We report the successful, low temperature synthesis of pure and Fe-doped titania nanoparticle (NP) powders, using organic Ti- and Fe- precursors. The properties of the synthesized titania based materials were obtained using XRD, UV/Vis and EPR spectroscopy and BET measurements. The doping of TiO_2 induced a shift in the absorption threshold towards the visible spectral range, compared to pure titania. The process of annealing induced an increase in crystallinity and particle sizes in theobtained materials. The photocatalytic activity, using simulated Solar light (Vitalux

lamp), of our samples was checked by following the photodegradation reaction of Rhodamine B and trichlorophenole as model compounds.

Keywords

Titania, x-ray diffraction, optical properties, textural properties, EPR, photocatalysis

1. INTRODUCTION

During recent decades, semiconductor based photocatalysis has been extensively studied and has become one of the most promising methods in environmental protection procedures such as air and water purification, hazardous waste remediation, and so on[1-3]. In the photocatalysis that is the subject of this paper, the semiconductor absorbs photons with sufficient energy (equal to or higher than the band-gap energy) which leads to the creation of electrons and holes that can initiate the reduction and/or oxidation of molecules adsorbed on its surface. Among various semiconductor photocatalysts, titanium dioxide (TiO_2) is particularly interesting due to its high efficiency, biological and chemical stability, non-toxicity and low cost [1-3]. However, it has some drawbacks such as the relatively high value of the band gap energy (about 3.2 eV), which limits its absorption to the UV spectral region, and the high recombination rate of photo induced electrons and holes, which decreases its photocatalytic activity. If we want to use solar light for photocatalysis in order to lessen the expenses of environmental remediation, the former drawback (E_g= 3.2 eV) is limiting because the content of UV light in the solar spectrum is about 5%. The improvement of TiO_2 visible-light activity is therefore the subject of extensive research in this field. The photocatalytic activity of TiO_2 can be improved by doping with metal

ions, such as nickel, chromium, iron, vanadium, zinc and others [1, 4]. These dopants create dopant states in the band gap of TiO_2 which can shift the absorption edge of TiO_2 towards the visible light region. Some experimental results have also shown that the incorporation of Fe-ions in TiO_2 crystal structure can do both: they narrow the band gap of TiO_2, and reduce the electron-hole recombination rate and thereby increase the photocatalytic efficiency of TiO_2 using visible light [5 - 8]. Numerous investigations have shown that the photocatalytic activity of Fe-doped TiO_2 is strongly dependent on the dopant concentration; higher contents of Fe^{3+} usually result in an increase in the recombination rate of photogenerated electrons and holes and thus a decrease in the photocatalytic activity [6-14]. If the iron concentration exceeds the optimal level, the Fe^{3+} ions steadily become the recombination centres of photogenerated electrons and holes. This has been ascribed to the fact that more Fe^{3+} sites trap more photogenerated electrons and holes, but the trapped free carrier pairs easily recombine through quantum tunnelling [10]. Thus, a higher Fe^{3+} content in the catalyst makes the recombination reaction more probable.

The photocatalytic activity of TiO_2 strongly depends on its structural properties, such as its crystalline structure and phase content. Titanium dioxide exists in three main crystallographic forms: anatase, rutile and brookite, with band gap energies of 3.2, 3.02 and 2.96 eV, respectively [15]. Anatase and rutile have a tetragonal crystal structure and they are widely used for photocatalytic applications. Brookite has an orthorhombic crystal structure and it is the least studied titanium dioxide phase [16]. The rutile form is the most stable polymorph of TiO_2, while the anatase and brookite forms are metastable and transform irreversibly to rutile at elevated temperatures [16, 17]. However, it is well known that anatase TiO_2 generally shows higher photoactivity then the rutile TiO_2 while

mixtures of these two phases show better photocatalytic activity than the pure versions [16, 18, 19]. From the data presented by Hurum and co-authors [18], mixed-phase titania catalysts show greater photoeffectiveness due to three factors: (1) the smaller band gap of rutile extends the useful range of photoactivity into the visible region; (2) the stabilization of charge separation by electron transfer from rutile to anatase slows recombination; (3) the small size of the rutile crystallites facilitates this transfer, creating catalytic hot spots at the rutile/anatase interface. This process depends critically on the interface between the TiO_2 phases and particle size. Additionally, if there are several anatase surface states related to oxygen vacancies, photoinduced electron transfer from the anatase surface states to rutile can occur, inducing photocatalytic reactions under visible light irradiation [19].

In the present work, pure and Fe-doped TiO_2 samples were synthesized using organic precursors, via the sol-gel method and characterized using various techniques: UV/Vis and EPR spectroscopy, X-ray diffraction and BET. The photocatalytic activity of pure and Fe-doped TiO_2 samples was tested using a degradation reaction of model compounds, before and after the heat treatment in order to investigate the influence of doping with Fe-ions as well as crystallinity and the crystalline structure (heat treatment) on their photocatalytic activity. In photocatalytical degradation reactions Rhodamine B and 2, 4, 6-trichlorophenol were used as model pollutants introduced in the environment mainly through the chemical industry (thanks to the manufacture of pharmaceuticals, dyes, pesticides, and the chlorination of municipal waters) [20]. These two model compounds will also be used for the evaluation of the influence of the chemical structure of the substrate on the photocatalytic activity of TiO_2.

Hence, the current analysis aims to study the low temperature synthesis of TiO_2 and Fe doped TiO_2 nanopowders by a low-cost method, and to understand the correlation between the structural, morphological and optical properties of pure TiO_2 and Fe doped TiO_2 nanopowders.

2. Methods and Materials

The following commercial reagents were used: Titanium(IV) isopropoxide (Aldrich, ≥97%), Iron(III) acetylacetonate (Aldrich, 99.9+%), Rhodamine B (RB, Sigma, ≈95%), 2,4,6-trichlorophenol (TCP, Alpha Aesar, 98%), nitric acid (J.T. Baker, 65%) and isopropanol (J.T. Baker, >99.8%). Degussa (D) was used as a reference material in the photodegradation study. All the chemicals were used as received. In all the experiments deionized water from Mili Q system was used.

2.1. Sample preparation

Both pure and Fe-doped TiO_2 samples were synthesized using the slightly modified synthetic procedure previously established by Wang et al [11]. In brief, 0.0975g of Iron(III) acetylacetonate was dissolved in 500 cm^3 of solvent mixture (water: isopropanol=1:1, pH≈2 adjusted by HNO_3), at 0ºC. Then, a solution of 4 cm^3 titanium(IV) isopropoxide in 20 cm^3 isopropanol was added dropwise under vigorous stirring. After 15 minutes at T=0ºC, the ice bath was removed and the reaction mixture was continuously stirred at room temperature for 48 hours. The resulting white dispersion was dialyzed against water until pH=6 was reached, then centrifuged (4000 rpm, 30 min) and dried until a constant weight at 75 ºC. Thereafter, the samples obtained were dispersed in an appropriate amount of water, continuously stirred at room

temperature overnight, centrifuged and dried again. This additional cleaning step was undertaken in order to remove possible organic residues from the sample surfaces. In the case of the undoped sample, the synthesis was performed in the same way but without the addition of iron (III)-acetylacetonate. In order to investigate the influence of the heat treatment/crystallinity and crystal structure of the samples on their photocatalytic activity, both pure and doped samples were annealed at 500ºC for 4h. The prepared samples were assigned as T1 (pure TiO_2) and FT1 (Fe-doped TiO_2) while the annealed samples were T2 and FT2.

2.2. Photocatalyst characterization:

The UV/Vis absorption and reflectance spectra of the pure and Fe-dopped TiO_2 powders were obtained using an Evolution 600 spectrophotometer (Thermo Scientific).

The XRD powder patterns were obtained by using a Philips PW 1050 powder diffractometer with Ni filtered Cu K_α radiation (λ = 1.5418 Å). The diffraction intensity was measured using the scanning technique (a step size of 0.05° and a counting time of 50 s per step).

The EPR spectra were recorded at room temperature using a Bruker Elexsys E540 EPR spectrometer operating at X-band (9.51 GHz) with the following settings: modulation amplitude, 2 G; modulation frequency, 100 kHz; microwave power, 10 mW and scan range, 6500 G. The spectra were recorded and analyzed using Xepr software (Bruker BioSpin). The samples were drawn into 5 cm long Teflon tubes (with wall thickness 0.025 mm and internal diameter 0.6 mm; Zeus industries, Raritan, USA). The measurements were performed using quartz capillaries into which Teflon tubes were placed.

The quantitative chemical analysis of the obtained nanomaterials was realized by inductively coupled plasma optical emission spectroscopy (ICP–OES) (Spectroflame ICP, 2.5 kW, 27 MHz). The measurements were performed by measuring the intensity of the radiation emitted by each element at a specific wavelength. The percentage of Fe-ions incorporated into the Fe-doped TiO_2 sample was analysed by ICP elemental analysis. The results obtained revealed that the actual percentage of Fe^{3+} ions incorporated into the TiO_2 structure is about 0.12%, which is significantly lower than the initially added amount of 2.5%, and in pure TiO_2 the concentration of Fe^{3+} ions was below the detection limit.

The textural properties of our samples were determined using nitrogen adsorption/desorption parameters. The nitrogen adsorption was performed at -196 °C and a relative pressure interval between 0.05 and 0.98 in automatic adsorption apparatus (Sorptomatic 1990 Thermo Finningen). Before each measurement, the sample was degassed at 200 °C under a vacuum for enough time (4 h < t < 10 h) to observe the absence of significant changes in vacuum stability. The adsorbed amount of nitrogen was measured by volume at standard temperature and pressure. The specific surface areas S_{BET} and C were calculated using the BET method [21-23] from nitrogen adsorption - desorption isotherms, using data up to $p/p_o = 0.3$, and the pore size distribution was computed from the desorption branch of the isotherms [23].

2.3. Photodegradation procedure:

The photocatalytic degradation procedure was carried out as follows: at atmospheric pressure and room temperature, 20 mg of the catalyst was added in 40 cm^3 of RB or TCP aqueous solution (concentrations: 5 x 10^{-5} and 5 x 10^{-4} mol/dm^3, respectively).

Before illumination, the mixture was stirred in the dark for one hour in order to achieve adsorption-desorption equilibrium. The reaction suspension was constantly bubbled with O_2 and magnetically stirred during irradiation. The suspensions were placed into a vessel which was exposed to white light from an Osram Vitalux lamp (300W, Sunlight simulation, white light: UVB radiated power from 280-315 nm 3.0W; UVA radiated power 315-400 nm 13.6W; the rest is visible light and IR). Optical power was measured using a R-752 Universal Radiometer read out with a model PH-30 sensor, DIGIRAD and it was ~ 30 mW cm^{-2} at a distance of 30 cm from the experimental solutions (used in this study) [24]. Aliquots (1 cm^3) were taken from the suspension and centrifuged.

2.4. Analytical procedure

For kinetic studies of RB and TCP photodegradation, using UV/Vis spectroscopy and liquid chromatography with diode array detection (HPLC), aliquots (1 cm^3) of the reaction mixture were taken at the beginning of the experiment and at regular time intervals. Each aliquot was then centrifuged. The supernatants were separated and the UV/Vis spectra were measured when degradation of RB was followed. RB has a characteristic peak in the UV/Vis spectra with a maximum at 549 nm, and absorptions were used as a RB concentration measurement due to the Lambert-Beer Law. Aliquots extracted from the TCP/ catalyst suspensions were diluted with 1ml of methanol and filtered through a Agilent Technologies Econofilter 25/0.2 μm PTFE (syringe filter). The absence of TCP adsorption on the filter was preliminarily checked.

After that, a 10 μL sample was injected and analyzed on an UltiMate 3000 HPLC System, equipped with a UV–Vis DAD set at the characteristic wavelength of the absorption maximum of TCP (292 nm), and a Hypersil GOLD (250 mm × 4.6 mm i.d.,

particle size 5 μm, 21◦C) column. The mobile phase (flow rate 1 cm^3/min) was a mixture of methanol and water (70 : 30, v/v). In repeated runs, the results agreed within 5–10%.

3. Results and Discussion

3.1. Structural properties of photocatalysts

Powder X-ray diffraction (XRD) analysis was used to identify the crystal phase and crystallinity of the prepared samples. The XRD patterns of the pure and Fe-doped TiO_2 samples before and after heat treatment are shown in Fig. 1a and b, respectively. X-ray diffractograms of all the prepared samples have observable maxima at 2θ values: 25.3, 37.8, 48, 53.9, 55.1, 62.7 and 68.8 deg., that are characteristic for the anatase phase (JCPDS 21-1272) [12, 25, 26]. Before the heat treatment, both samples have an anatase crystal structure with a small additional content of brookite phase (B peak at 30.8°, JCPDS 29-1360) [27]. No separate dopant related peaks were found in the X-ray diffractograms of the Fe-doped TiO_2 samples, which indicates that the Fe ions are fully incorporated into the TiO_2 lattice, as expected due to the ionic radii of Ti^{4+} and Fe^{3+} , 0.605 Å and 0.64 Å respectively [28]. After heat treatment, both samples mainly kept an anatase crystalline structure with the addition of a brookite phase, though a small amount of the rutile structure appears as well (JCPDS 21-1276) [5, 12]. The calculated content of the rutile phase is about 7 % for pure and about 10% for Fe-doped TiO_2 sample, according to XRD measurements and the Spurr equation [29]; the brookite content in the all samples is about 2%.

The average crystallite size (D in nm) was determined from XRD spectra according to the Scherrer equation (1):

$$D = \frac{k\lambda}{\beta cos\theta} \quad (1)$$

where k is a constant equal to 0.89, λ is the X-ray wavelength equal to 0.15418 nm, β is the full width at half maximum intensity (FWHM) of the (101) peak and θ is the diffraction angle (rad). The calculated values of the crystallite sizes of the samples showed that annealing induced a small increase in crystalline domain sizes, from 4 to 14 nm for pure and from 7 to 10 nm for doped samples, together with increased crystallinity. The presence of Fe ions can induce the formation of larger particles when higher concentrations are present and a reduction of Fe^{3+} to Fe^{2+} can be expected. The ionic radius of Fe^{2+} is 0.78 Å, much larger than the radius of Ti^{4+} (0.605 Å) [28].

Figure 1. The XRD patterns of pure (a) and Fe-doped (b) TiO_2 powders.

Doping with Fe ions, and other ions as well, has an influence on the average crystallite size, most probably because the incorporation of Fe ions into TiO_2 particles can lead to a certain deformation of the TiO_2 crystal unit cell. After heat treatment, the size differences between pure and doped particles were preserved. The effect of the different dopants on the anatase - rutile transformation and stability has already been reported [13, 17]. For example, in the case of nitrogen doped TiO_2 nanoparticles, an inhibition of the structural transition is observed with the introduction of nitrogen ions into the anatase structure, in spite of the opposite effect associated with the contribution of oxygen vacancies induced by the nitrogen incorporation. On the other hand, it is well known that an increase in the size of particles also favours the structural transition due to the different surface energy [13].

3.2. Optical properties of photocatalysts

The optical properties of the prepared samples were investigated using UV-Vis reflectance spectroscopy. Figure 2a shows the UV-Vis diffuse reflectance spectra of the pure and Fe-doped TiO_2 samples before and after heat treatment. For the undoped sample, a typical TiO_2 DRS curve was obtained with a broad absorption band below 400 nm. However, when Fe^{3+} ions were present in the sample, a clear red shift was observed characterized by the occurrence of a sub-band gap absorption tail in the visible range. It can be seen that the spectral response of the doped TiO_2 sample and both the pure and Fe-doped annealed samples is shifted towards visible spectral region compared to the pure, as prepared TiO_2. The reflectance spectra were analysed using the Kubelka-Munk method. Using the calculated values, Tauc`s plots (Figure 2b) were drawn in order to estimate the band gap energies of the prepared samples (a plot of $(F(R)\cdot h\nu)^{1/2}$ versus photon energy ($h\nu$), where F(R) is the Kubelka-Munk function). The estimated band-gap energies are summarized in Table 1.

As already stated, it was found that the incorporation of Fe ions into the titania matrix forms sub-band states in the band gap of TiO_2 [5, 6]. The reflection spectra of the doped samples are characterized by a shoulder between 450 and 500 nm and the intensity increases with annealing. Its existence can be assigned to either the d–d transition of the $_2T^{2g}$-$_2A^{2g}$ and $_2T^{2g}$-$_2T^{1g}$ of Fe^{3+} or the charge transfer transition between iron ions ($Fe^{3+} + Fe^{3+} \rightarrow Fe^{2+} + Fe^{4+}$) [5]. Along with the incorporation of Fe ions, oxygen defect band states are also formed in the band gap. In chemically pure TiO_2, the electronic transition occurs directly from valence to the conduction band. However, on doping, the electrons are not directly excited into the conduction band since the unoccupied dopant electronic states and oxygen vacancies capture the electrons. The charged oxygen defect states

formed in TiO_2 are F (two electrons), F^+ (single electron), and F^{++} (devoid of electrons) [30]. The oxygen vacancy states that may capture electrons are F^+ and F^{++}, respectively. Therefore, the sub-band states of Fe ions and the oxygen defects are responsible for the reduction of the effective band gap of TiO_2 nanoparticles. The transitions involved in the observation of the absorption tails in the visible region (as can be seen in Fig. 2a and 2b) are usually described by the following equation:

$$\alpha = \alpha_0 \exp\left(\frac{h\upsilon}{E_u}\right) \quad (2)$$

where α is absorption coefficient, (hν) is the photon energy and E_u corresponds to the so-called Urbach energy. E_u is correlated to the transitions between intra-gap levels and the energy levels in the valence or conduction bands. Thus, according to Eq. (2), the reciprocal of the slope of the plot of ln(F(R)) as a function of the energy (hν), as presented in Figures 2c-f, leads to E_u [31]. The obtained E_u values for the analysed nanoparticles are displayed in Table 1. The reduction in the band-gap energy due to the annealing of Fe doped sample (Table 1, FT1 and FT2) has been associated with a clear increase in E_u, as suggested by Chundhury and Chundhury [32]. The opposite trend, although small, in E_g and E_u has been observed for chemically pure TiO_2 due to the different origin of absorption tailing; in pure titania. oxygen vacancies are predominately responsible for tailing. Annealing titania in an air atmosphere induce the crystallization and saturation of titania with oxygen. The small decrease in the band gap can be assigned to the formation of the rutile crystalline phase, while the brookite phase was present in the prepared samples as well.

To summarize, UV-Vis results have shown that the incorporation of Fe-ions into the TiO_2 structure, as well as heat treatment, decreased the band-gap energy of TiO_2 nanoparticles. This can be explained by the formation of dopant energy levels within the

band gap of TiO_2 [5 - 12]. The results obtained also indicated that heat treatment decreased the band gap energies of both the pure and Fe doped TiO_2 samples. The decrease in band gap energy may be due to the increase of rutile crystalline phase content in the nanoparticles, as is indicated by XRD results (Fig. 1).

Table 1. Calculated values of band-gap (E_g) and Urbach (E_u) energies.

Sample	E_g (eV)	E_u (meV)
T1	3.1	210
T2	3.0	198
FT1	2.8	181
FT2	2.3	256

Figure 2. (a) UV-Vis diffuse reflectance spectra, (b) Tauc's plots and (c, d, e, f) plots used for the determination of Urbach energies of titania samples.

3.3. Electron paramagnetic resonance spectroscopy (EPR)

Since EPR is sensitive to various kinds of structural defects, like oxygen vacancies present in the material, this resonance technique was used to identify the defects in pure and Fe doped annealed TiO_2 NPs (Figure 3). By calculating the g factor (EPR parameter), it is possible to get information about the type of oxygen defects, using the following equation [33]:

$$g = \frac{h\nu}{\mu_B H} \quad (3)$$

where H is the magnetic field (T), ν is the frequency (Hz, s^{-1}), μ_B is the Bohr magneton equal to 9.274 x 10^{-24} J/T and h is Planck's constant, 6.626 x 10^{-34} J s.

Figure 3. Room temperature EPR spectra of pure and Fe-doped annealed TiO_2.

In Figure 3, the EPR spectra of pure and Fe-doped annealed TiO_2 are presented. The spectrum of Fe-doped TiO_2 consists of two main signals at g ~ 2.0 and at g ~ 4.3. Both peaks can be assigned to Fe^{3+} ions. The signal at g ~ 2 is related to Fe^{3+} ions in the anatase bulk lattice, substituting Ti^{4+}, in octahedral symmetry, which interact with each other through oxygen vacancies [8, 30-33]. The signal at g ~ 4.3 can be related to Fe^{3+} isolated cations in a rhombic environment, attributable to the presence of oxygen vacancies in the anatase-like close environment of the cations [9, 33]. Additionally, it can be attributed to the Fe^{3+} ions dispersed on the surface of the TiO_2 nanoparticles [8, 14]. The spectrum of pure TiO_2 NPs has less a intensive spectrum compared to the doped sample. The signal at g ~ 2 can be assigned to oxygen vacancies in pure TiO_2 [33]. The obtained EPR results indicate that the Fe ions were successfully incorporated into the TiO_2 matrix, with a distribution of ions both on the surface and in the bulk.

3.4. Textural properties

Both the pure and Fe doped annealed samples are characterized by a type IVa isotherm with a hysteresis loop of the H2 type, as can be seen in Figure 4a, indicating the presence of mesopores, within the well-defined pore shape type [21-23]. The sharp steps in the isotherms suggest that capillary condensation occurs in a narrow range of

mesopores. A type IVa isotherm is encountered when adsorption occurs on low porosity material or on material with generally mesoporous pore diameters. The mesoporosity is characterized by the capillary condensation step in the isotherm between the relative pressures of 0.5 and 0.8.

Figure 4. (a) N_2 adsorption/desorption isothermes and (b) pore size distribution (D is diameter of the pore) of pure and Fe doped, annealed TiO_2.

The textural properties of the annealed samples are given in Table 2

Table 2. Textural properties of annealed photocatalysts.

Sample	S_{BET}, m^2g^{-1}	D_{max}, nm	V,cm^3g^{-1}
T2	49	5.4	0.092
FT2	74	4.6	0.109

As can be seen in Table 2, and in Figure 4, the addition of Fe to the TiO_2 slightly improve the textural properties of the TiO_2 and causes a shift in the D_{max} of mesopores towards the micropore range.

3.5. Photodegradation properties

The photocatalityc activity of our titania samples and Degussa, was examined by studying the degradation of RB and TCP under UV-Vis light irradiation, being simulated Solar light. Figures 5a and b show the photocatalytic degradation of RB in the presence of pure and Fe-doped TiO_2 before and after the heat treatment. The concentration ratios, presented as C/C_0 (where C_0 is the concentration at zero time and C is the concentration at the time t of irradiation) were plotted as a function of the irradiation time. In Figure 5a, the direct photolysis of Rhodamine B under UV-Vis light irradiation is also presented ,which is almost negligible. As can be seen, the photocatalytic activity of pure and Fe-doped TiO_2 was almost the same before annealing. The process of heat treatment induced changes in the photocatalytic activity: the activity of pure TiO_2 was significantly increased, but the activity of Fe-doped titania was decreased compared to the as prepared samples. These findings indicated that the heat treatment strongly influences not only the structure (Figure 1) but also photoactivity of the TiO_2 nanoparticles. XRD measurements have shown that the pure TiO_2 sample before heat treatment has a predominantly anatase crystalline structure with a small additional content of the brookite phase, while after the heat treatment sample kept a mixture of the anatase and brookite crystalline structures, and a small amount of the rutile structure appears. The enhanced photocatalityc activity of the heat treated TiO_2 sample can be attributed to the proper phase composition of the sample i.e. the proper rutile to anatase ratio in the sample. As can be found in the literature [18], the presence of a small content of the rutile phase close to the anatase phase creates a structure where rapid electron transfer from the rutile to the anatase occurs, and vice

versa, depending on the photon energy, due to the position of the energy bands and trapping sites of anatase and rutile. Hurum et al. [18] attributed the high catalytic activity of mixed-phase TiO_2 catalysts in large part to this synergistic activation of the rutile phase by anatase. The rutile phase extends the photoactive range into the visible spectral range, harvesting more light, and the electron transfer from the rutile to anatase trapping sites hinders charge recombination [18]. In addition, the increase in crystallinity can be beneficial for photocatalytic activity [34].

Figure 5. (a) Kinetic plots of the photolysis and degradation of RB in the presence of Degussa (D), pure and Fe-doped TiO_2 before and after heat treatment; and (b) percentage of RB decomposed as a function of time of irradiation in the presence of prepared photocatalysts.

Figure 6. (a) Kinetic plots of the photolysis and degradation of TCP in the presence of Degussa (D), pure and Fe-doped annealed TiO_2 ; and (b) percentage of TCP decomposed as a function of time of irradiation in the presence of prepared photocatalysts.

The Fe-doped TiO_2 samples showed lower photocatalytic activity than the undoped samples after the heat treatment, although it has slightly higher specific surface area (Table 2) compared to pure annealed TiO_2. Possible causes of such behaviour could include an increased recombination rate of the photogenerated electrons and holes at the Fe^{3+} dopant centres [6, 12], a decreased number of active sites on the surface of TiO_2 or the different adsorption properties of active sites on the NPs surface. As

mentioned above, the incorporation of Fe-ions into the TiO_2 structure could narrow the band gap of TiO_2, reduce the electron hole recombination rate and thereby increase the photocatalytic activity of TiO_2 in the visible range. But it is necessary to achieve an optimal percentage of Fe-ions incorporated into the TiO_2 host in order to obtain the improved photocatalytic activity [6-9, 11, 12]. If the dopant concentration is not optimal, the dopant energy levels incorporated within the band gap of TiO_2 may become effective recombination centres for the photogenerated electron and holes. On the other hand, Fe-ions can cover the active sites on the surface of TiO_2 nanoparticles and, consequently, decrease their photocatalytic activity. In addition, XRD measurements have shown that the incorporation of Fe-ions into the TiO_2 crystal structure, and agglomeration during the heat treatment, result in an increase in the crystallinity and crystallite size and a small content of the rutile phase can be observed. Here, the synergistic effect between anatase and rutile is not sufficiently significant to prevent recombination at the Fe-ions incorporated into the crystal matrix.

In order to correlate the photocatalytic activity of titania powders with the molecular structure of the pollutant, we followed the degradation of TCP as well. The kinetic curves of TCP degradation in the presence of annealed catalysts are presented in Figure 6a. Figure 6b shows the comparison of the photocatalityc activities of the catalysts used. As can be seen, for early stages of irradiation, the best results were obtained for annealed Fe-doped TiO_2 which was even better that Degussa. The differences between the photocatalytic activities of pure and doped TiO_2 are not as large as for RB (Figure 5), and most probably can be assigned to the different structures of pollutants (RB and TCP) and their different adsorption affinities regarding titania surfaces. We obtained similar differences between results when we studied the photocatalytic activity of Fe-

doped rutile and N-doped anatase regarding the degradation of different herbicides [6]. The best photocatalyst for the degradation of one herbicide was not the best one for the other and it seems that there is still a need for the development of new methods for the synthesis of TiO_2 and for its modification (mixtures of different crystal phase, doping with cations and anions, surface modification and so on). Doped and annealed titania was even more efficient than Degussa for the first 90 min of irradiation but for longer irradiation times Degussa showed better results (Figure 6b). The synthesized titania catalysts behaved as though a kind of saturation took place for longer irradiation times, and after 90 min of irradiation, the rate of the degradation reaction decreased significantly, most probably because the intermediates started to degrade as well.

4. Conclusions

We used low temperature method for the synthesis of pure and Fe-doped TiO_2 nanoparticles from organometallic precursors. XRD analysis showed that the dominant structure was anatase, with a small content of the brookite phase. The process of annealing at 500°C induced an increase in both crystallinity and particle sizes, and the appearance of the rutile phase. UV/Vis reflectance spectroscopy revealed that Fe-doping moved the absorption threshold to lower energies compared to chemically pure titania. Tauc's plots were used to estimate the band gap energies of the titania samples, which were between 3.1 and 2.3 eV. In addition, tailing in the DRS spectra was assigned to oxygen vacancies and doping. Urbach energies, as a measure of transitions between defect levels and valence/conduction bands were calculated. The annealing of pure titania reduces E_u, while the annealing of the doped sample increases defect/dopant dependant absorption properties. EPR spectroscopy revealed that titania nanoparticles

were successfully doped with Fe^{3+} ions. The EPR results showed that Fe^{3+} ions were distributed in the bulk anatase lattice by substituting Ti^{4+} in octahedral symmetry (g ~ 2) and the presence of isolated Fe^{3+} ions on the TiO_2 nanoparticle surface (g ~ 4.3). Evaluation of the photodegradation properties showed that best photocatalyst for the degradation of RB is annealed pure TiO_2, while for the degradation of TCP it is annealed doped catalyst, which was more effective than Degussa during first 90 min of irradiation.

Acknowledgement

Financial support for this study was granted by The Ministry of Education, Science and Technological Development of The Republic of Serbia, Projects: 172056, 172015 and 45020.

References

[1] J. Schneider, M. Matsuoka, M. Takeuchi, J. Zhang, Y. Horiuchi, M. Anpo, D.W. Bahnemann, Understanding TiO_2 photocatalysis: mechanisms and materials, Chem. Rev. **114** (2014) 9919-9986.

[2] A. Fujishima, T. Rao, D.A. Tryk, Titanium dioxide photocatalysis, J. Photoch. Photobio. C **1** (2000) 1-21.

[3] H. Xu, S. Ouyang., L. Liu, P. Reunchan, N. Umezawa, J. Ye, Recent advances in TiO_2-based photocatalysis, J. Mater. Chem. A **2** (2014) 12642-12661.

[4] J. Choi, H. Perk, M.R. Hoffmann, Effects of single metal-ion doping on the visible-light photoreactivity of TiO_2, J. Phys. Chem. C **114** (2010) 783-792.

[5] N.D. Abazović, M.I. Čomor, S. Zec, J.M. Nedeljković, E. Piscopiello, A. Montone, M. Vittori Antisari, Structural and optical characterization of flower-like rutile nanostructures doped with Fe^{3+}, J. Am. Ceram. Soc. **92 (4)** (2009) 894-896.

[6] D.V. Šojić, V.N. Despotović, N.D. Abazović, M.I. Čomor, B.F. Abramović, Photocatalytic degradation of selected herbicides in aqueous suspensions of doped titania under visible light irradiation, J. Hazard. Mater. **179** (2010) 49-56.

[7] S. Manu, M. Abdul Khadar, Non-uniform distribution of dopant iron ions in TiO_2 nanocrystals probed by X-ray diffraction, Raman scattering, photoluminescence and photocatalysis, J. Mater. Chem. C **3** (2015) 1846-1853.

[8] X. Lu, Y. Ma, B. Tian, J. Zhang, Preparation and characterization of Fe-TiO_2 films with high visible photoactivity by autoclaved-sol method at low temperature, Solid State Sci. **13** (2011) 625-629.

[9] C. Adan, A. Bahamonde, M. Fernandez-Garcıa, A. Martınez-Arias, Structure and activity of nanosized iron-doped anatase TiO_2 catalysts for phenol photocatalytic degradation, Appl. Catal. B-Environ. **72** (2007) 11–17.

[10] Z.B. Zhang, C.C. Wang, R. Zakaria, J.Y. Ying, Role of particle size in nanocrystalline TiO_2-based photocatalysts, J. Phys. Chem. B **102** (1998) 10871–10878.

[11] C. Wang, D.W. Bahnemann, J. Dorhmann, A novel preparation of iron-doped TiO_2 nanoparticles with enhanced photocatalytic activity, Chem. Commun (2000) 1539-1540.

[12] N.D. Abazović, L. Mirenghi, I.A. Janković, N. Bibić, N. Šojić, B.F. Abramović, M.I. Čomor, Synthesis and characterization of rutile TiO_2 nanopowders doped with iron ions, Nanoscale Res. Lett. **4** (2009) 518-525.

[13] S. Larumbe, M. Monge, C. Gómez-Polo, Comparative study of (N, Fe) doped TiO_2 photocatalysts, Appl. Surf. Sci. **327** (2015) 490–497.

[14] X. Li, P.L. Yue, C. Kutal, Synthesis and photocatalytic oxidation properties of iron doped titanium dioxide nanosemiconductor particles, New J. Chem. **27** (2003) 1264–1269.

[15] S.M. Gupta, M. Triptahi, A review of TiO_2 nanoparticles, Chinese Sci. Bull. **56** (2011) 1639-1657.

[16] A. Di Paola., M. Bellardita, L. Palmisano, Brookite, the Least Known TiO_2 Photocatalyst, Catalysts **3** (2013) 36-73.

[17] D. A. Hanaoar, C.C. Sorrell, Review of the anatase to rutile phase transformation, J. Mater. Sci. **46** (2011) 855-874.

[18] D.C. Hurum, A.G. Agrios, K.A. Gray, T. Rajh, M.C. Thurnauer, Explaining the enhanced photocatalytic activity of Degussa P25 mixed-phase TiO_2 Using EPR, J. Phys. Chem. B **107** (2003) 4545-4549.

[19] L. Jing, S. Li, S. Song, L. Xue, H. Fu, Investigation on the electron transfer between anatase and rutile in nano-sized TiO_2 by means of surface photovoltage technique and its effects on the photocatalytic activity, Sol. Energ. Mat. Sol. C **92** (2008) 1030-1036.

[20] S. Sood, A. Umar, S.K. Mehta, S.K. Kansal, α-Bi_2O_3 nanorods: An efficient sunlight active photocatalyst for degradation of Rhodamine B and 2,4,6-trichlorophenol, Ceram. Int. **41** (2015) 3355-3364.

[21] F. Rouquerol, J. Rouquerol, K.S.W. Sing, P. Llewellyn, G. Maurin, Adsorption by powders and porous solids, principles, methodology and applications, Academic Press, New York, 2012.

[22] B.C. Lippens, B.G. Linsen, J.H. de Boer, Studies on pore systems in catalysts I. The adsorption of nitrogen; apparatus and calculation, J. Catal. **3** (1964) 32-37.

[23] K. Sing, D. Everet, R. Haul, L. Moscou, R. Pierotti, J. Rouquerol, T. Siemieniewska, Reporting physisorption data for gas/solid systems, Pure Appl. Chem. **57** (1985) 603-619.

[24] M. Radoičić, Z. Šaponjić, I.A. Janković, G. Ćirić-Marjanović, S.P. Ahrenkiel, M.I. Čomor, Improvements to the photocatalytic efficiency of polyaniline modified TiO_2 nanoparticles, Appl. Cat. B: Environ. **136-137** (2013) 133-139.

[25] N.D. Abazović, M.I. Čomor, M.D. Dramićanin, D.J. Jovanović, S.P. Ahrenkiel, J.M. Nedeljković, Photoluminescence of anatase and rutile TiO_2 particles, J. Phys. Chem. B **110** (2006) 25366–25370.

[26] N.D. Abazović, I.A. Ruvarac-Bugarčić, M.I. Čomor, N. Bibić, S.P. Ahrenkiel, J.M. Nedeljković, Photon energy up-conversion in colloidal TiO_2 nanorods, Opt. Mater. **30** (2008) 1139–1144.

[27] J. Xu, Y. Ao, D. Fu, C. Yuan, Synthesis of Gd-doped TiO_2 nanoparticles under mild condition and their photocatalytic activity, Colloid. Surface. **334** (2009) 107-111.

[28] R.D. Shannon, Revised effective ionic radii and systematic studies of interatomic distances in halides and chalcogenides, Acta Crystallogr. A **32** (1976) 751–767.

[29] R.A. Spurr, H. Myers, Quantitative analysis of anatase-rutile mixtures with an X-ray diffractometer, Anal. Chem. **29** (1957) 760-762.

[30] N. Serpone, Is the band gap of pristine TiO_2 narrowed by anion and cation doping of titanium dioxide in second generation photocatalysts?, J. Phys. Chem. B **110** (2006) 24287–24293.

[31] B. Choudhury, M. Dey, A. Choudhury, Defect generation, d-d transition, and band-gap reduction in Cu-doped TiO_2, International Nano Letters **3 (**2013) 25.

[32] B. Choundhury, A. Choundhury, Oxygen defect dependent variation of band gap, Urbach energy and luminescence property of anatase, anatase-rutile mixed phase and of rutile phases of TiO_2 nanoparticles, Phys. E **56** (2014) 364-371.

[33] S.K.S. Patel, S. Kurian, N.S. Gajbhiye, Room-temperature ferromagnetism of Fe-doped TiO_2 nanoparticles driven by oxygen vacancy, Mater. Res. Bull., **48** (2013) 655–660.

[34] M.B. Radoičić, I.A. Janković, V.N. Despotović, D.V. Šojić, T.D. Savić, Z.V. Šaponjić, B.F. Abramović, M.I. Čomor, The role of surface defect sites of titania nanoparticles in the photocatalysis: aging and modification, Appl. Cat. B: Environ. **138-139** (2013) 122-127.

Table Captions

Table 1. Calculated values of band-gap (E_g) and Urbach (E_u) energies.

Table 2. Textural properties of annealed photocatalysts.

Figure Captions

Figure 1. The XRD patterns of pure (a) and Fe-doped (b) TiO_2 powders.

Figure 2. (a) UV-Vis diffuse reflectance spectra, (b) Tauc's plots and (c, d, e, f) plots used for determination of Urbach energy, of pure and Fe-doped TiO_2 samples before and after heat treatment.

Figure 3. Room temperature EPR spectra of pure and Fe-doped annealed TiO_2.

Figure 4. (a) N_2 adsorption/desorption isothermes and (b) pore size distribution of pure and Fe doped, annealed TiO_2.

Figure 5. (a) Kinetic plots of the degradation of RB in the presence of Degussa (D), pure and Fe-doped TiO_2 before and after heat treatment; and (b) percentage of Rhodamine B decomposed as a function of time of irradiation in the presence of prepared photocatalysts.

Figure 6. (a) Kinetic plots of the degradation of TCP in the presence of Degussa (D), pure and Fe-doped TiO_2 after heat treatment; and (b) percentage of TCP decomposed as a function of time of irradiation in the presence of prepared photocatalysts.

Figures

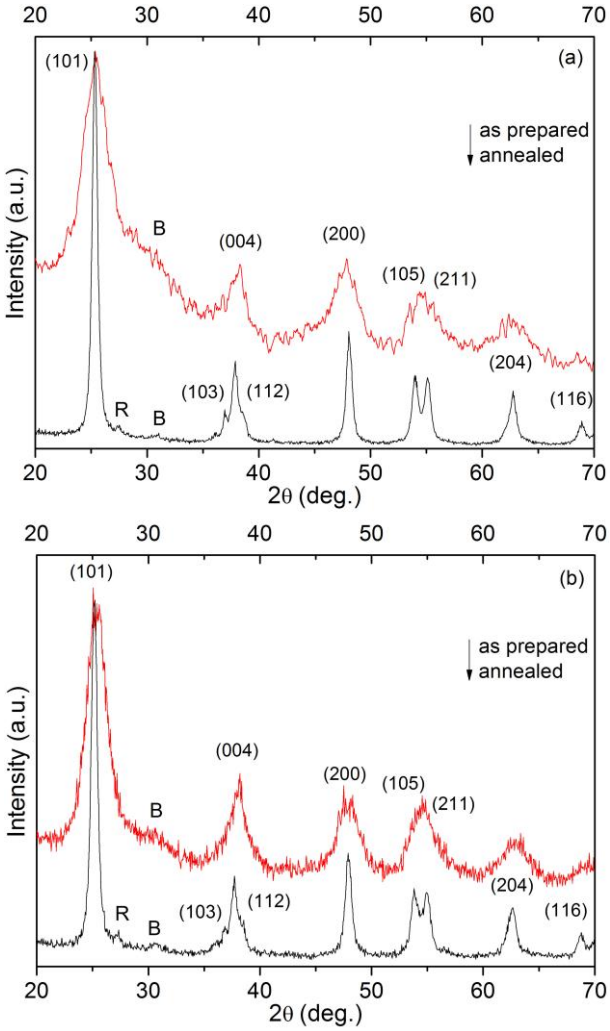

Fig. 1

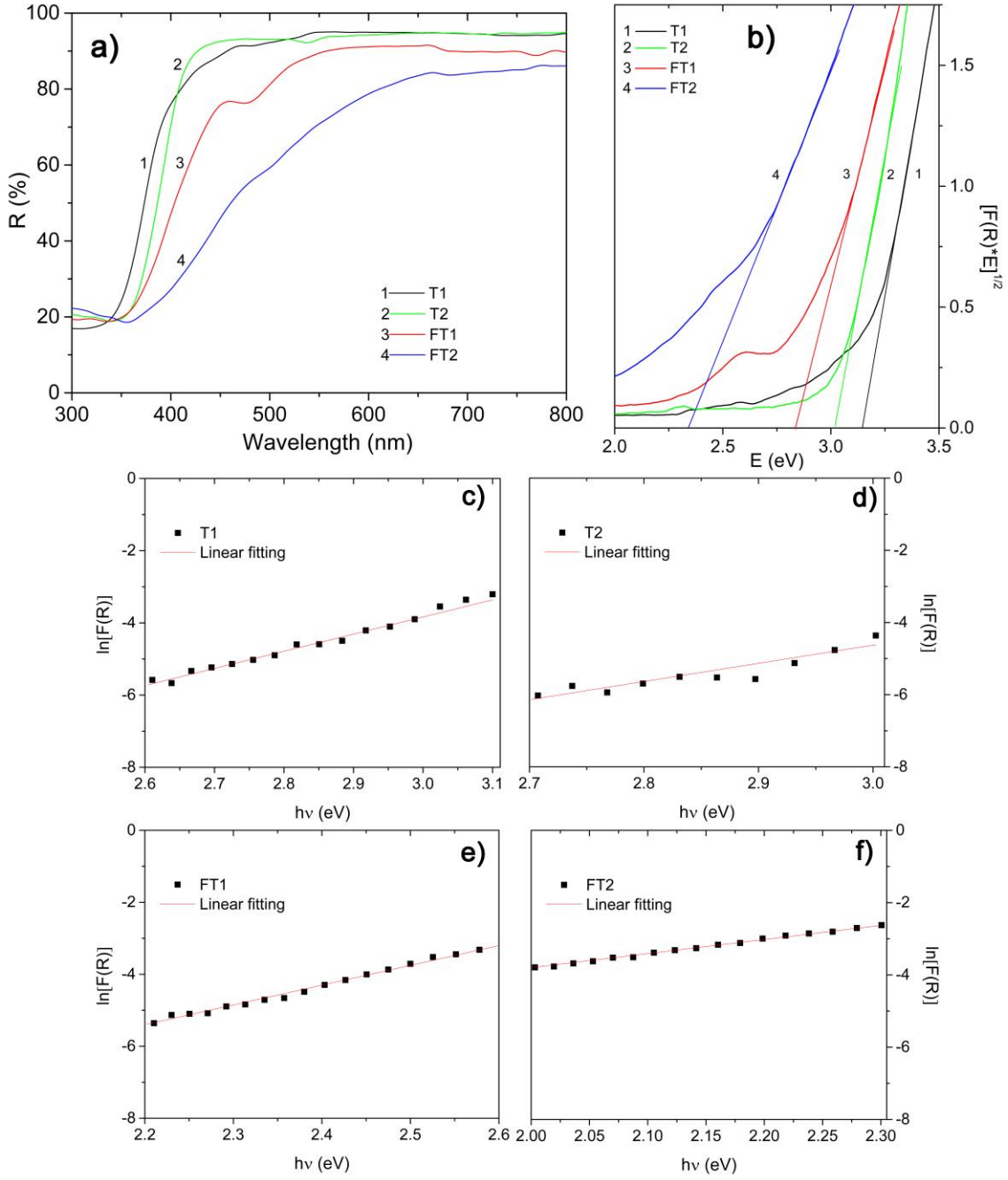
a)
R (%)
Wavelength (nm)
1 T1
2 T2
3 FT1
4 FT2
b)
[F(R)*E]^1/2
E (eV)
c)
T1
Linear fitting
ln[F(R)]
hν (eV)
d)
T2
Linear fitting
e)
FT1
Linear fitting
f)
FT2
Linear fitting

Fig. 2

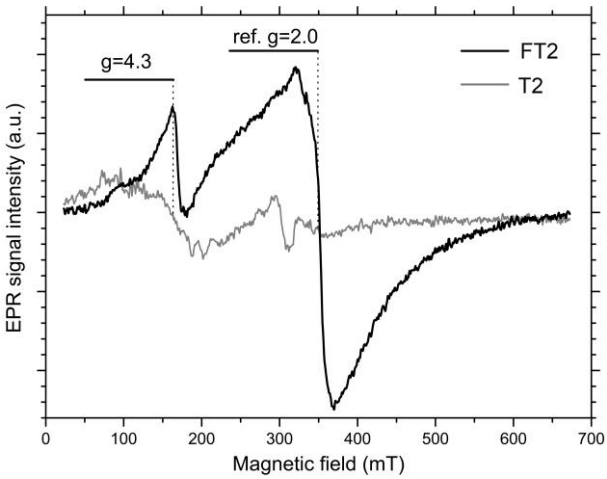
g=4.3
ref. g=2.0
FT2
T2
EPR signal intensity (a.u.)
0
100
200
300
400
500
600
700
Magnetic field (mT)

Fig. 3

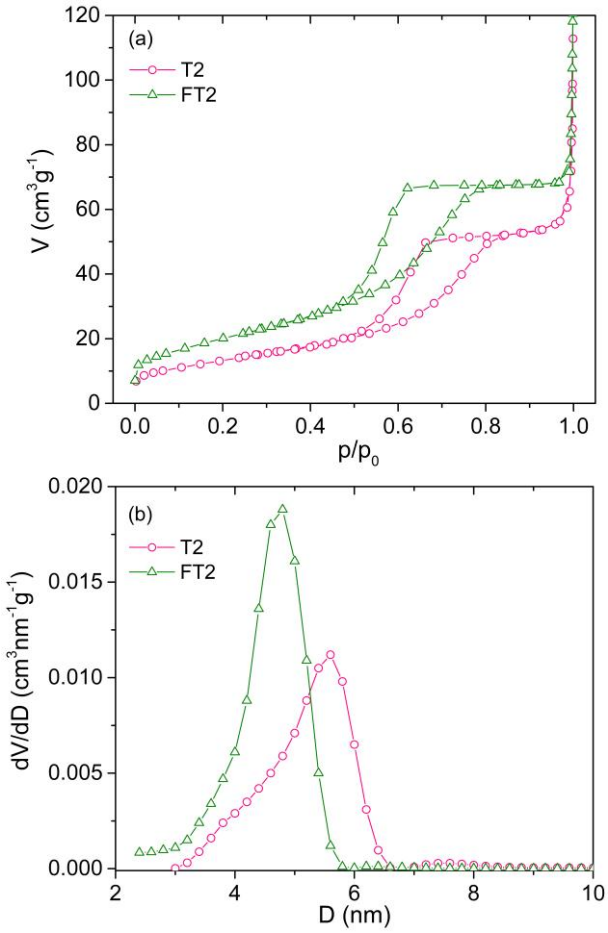
(a)
T2
FT2
V (cm3g-1)
0
20
40
60
80
100
120
0.0
0.2
0.4
0.6
0.8
1.0
p/p0
(b)
T2
FT2
dV/dD (cm3nm-1g-1)
0.000
0.005
0.010
0.015
0.020
2
4
6
8
10
D (nm)

Fig. 4

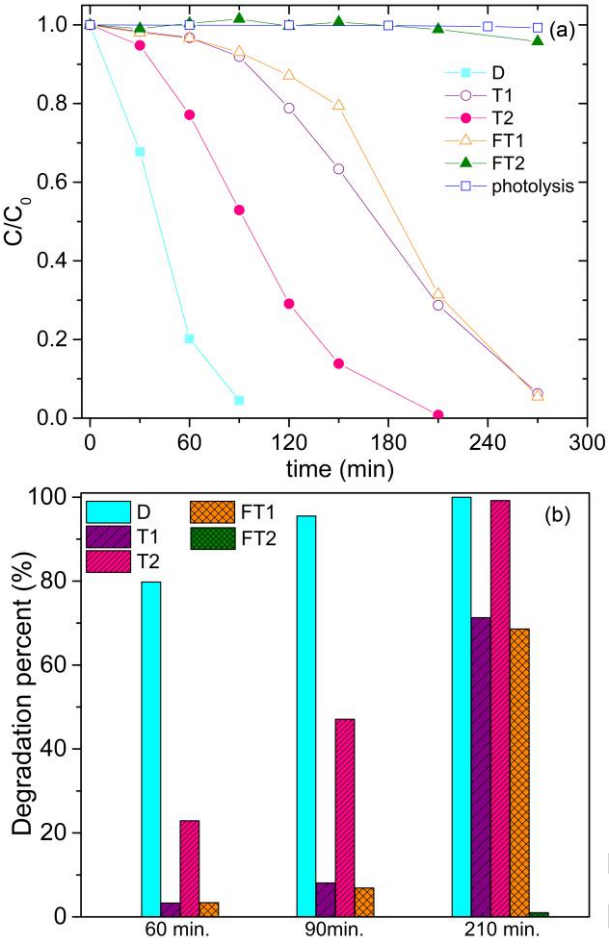

Fig. 5

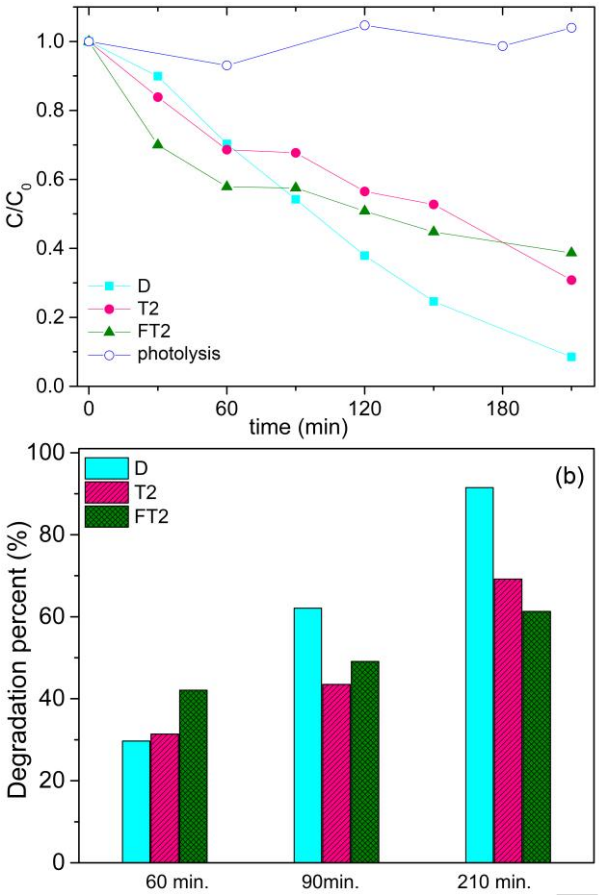

Fig. 6